J. Plasma Fusion Res. SERIES, Vol.7 (2006) 35-39

Modeling of Impurity Transport in High Density Plasma with Highly Enhanced Radiation Loss on JT-60U

TAKENAGA Hidenobu, ASAKURA Nobuyuki, KUBO Hirotaka, KONOSHIMA Shigeru, NAKANO Tomohide, PORTER Gary[1], ROGNLIEN Thomas[1] and RENSINK Marvin[1]

Japan Atomic Energy Research Institute, Naka 311-0193, Japan*

[1] *Lawrence Livermore National Laboratory, Livermore, CA 94551-9900, USA*

(Received: 5 October 2004 / Accepted: 20 May 2005)

Abstract

Impurity transport has been modeled using a 1-D transport code for the main plasma and a 2-D fluid code (UEDGE) for the divertor and scrape-off layer plasmas in the JT-60U high β_p mode plasma with highly enhanced radiation by injecting seed impurity argon. The density profile of the seed impurity argon estimated from the soft x-ray profile was more peaked by a factor of 2 than the electron density profile. On the other hand, the density measurement of the fully ionized intrinsic impurity carbon indicated a flat carbon density profile. The radiation profile evaluated from these impurity density profiles was more peaked than the measurement in the main plasma. The divertor radiation calculated by the UEDGE code with the boundary condition of the argon density consistent with the 1-D transport analysis was localized around the strike points compared with the measurement.

Keywords:

JT-60U, impurity transport, seed impurity, intrinsic impurity, 1-D transport code, UEDGE code, radiation profile

1. Introduction

Reduction of heat load localized onto the divertor plates is a critical issue in magnetic confined fusion devices to mitigate damage of the divertor plates. High radiation loss in the divertor and scrape-off layer (SOL) plasmas enhanced by injecting seed impurity is most effective for expansion of the heat load onto the wide area. In JT-60U, the high radiation loss operation has been developed with the seed impurity neon or argon [1], and the radiation loss power has reached to over 80 % of the net heating power in high density plasmas. In order to extrapolate these results to ITER and DEMO reactor, understanding of the impurity transport is important. The impurity transport has been analyzed using a 1-D transport code for the main plasma [2] and a 2-D fluid code [3] or a Monte-Carlo code [4] for the divertor and SOL plasmas. In these analyses, impurity density and/or transport coefficients were evaluated. However, detailed comparison of the radiation profile between modeling and experiment was not performed. In this paper, the impurity density was estimated using a 1-D transport code for the main plasma and the 2-D fluid code UEDGE [5] for the divertor and SOL plasmas in the high β_p mode plasma with highly enhanced radiation by injecting seed impurity argon. The radiation profile was calculated based on the estimated impurity densities for both seed impurity argon and intrinsic impurity carbon and it was compared with the measurement.

2. Experiments

JT-60U is a large tokamak device with a major radius of 3.4 m. The typical plasma configuration is shown in Fig. 1 together with sight lines of the diagnostics related to this study. The W-shaped divertor was adopted, where the inner and outer inclined divertor plates and the dome in the private flux region form a W-shaped surface. The divertor pumping was performed from both inner and outer private flux regions. The soft x-ray emission intensities were measured with 10 sight lines in the main plasma. The radiation loss was measured with 20 sight lines using bolometer arrays. 8 lines (ch 1-8) were arranged for the main plasma side and 12 lines (ch 9-20) were arranged for the divertor region.

The seed impurity of argon was injected into high density high β_p mode plasmas with an internal transport barrier (ITB) at the plasma current of I_p = 1.0

Corresponding author's e-mail: takenaga.hidenobu@jaea.go.jp
* *Present: Japan Atomic Energy Agency*

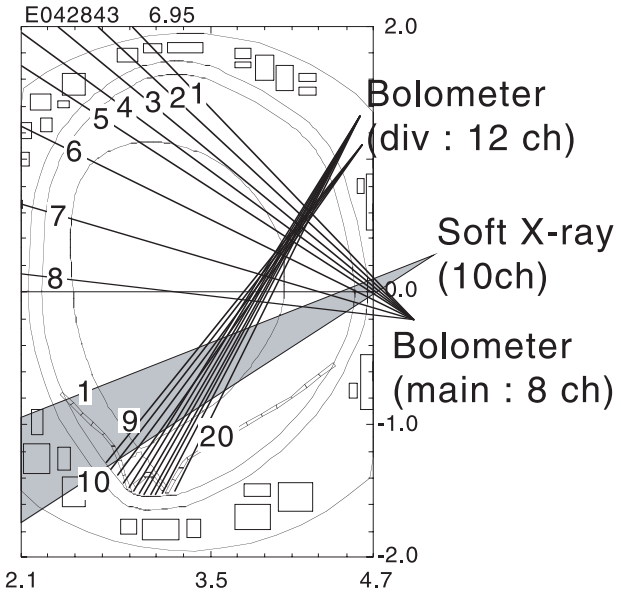

Fig. 1 Typical plasma configuration and diagnostic arrangements related to this study.

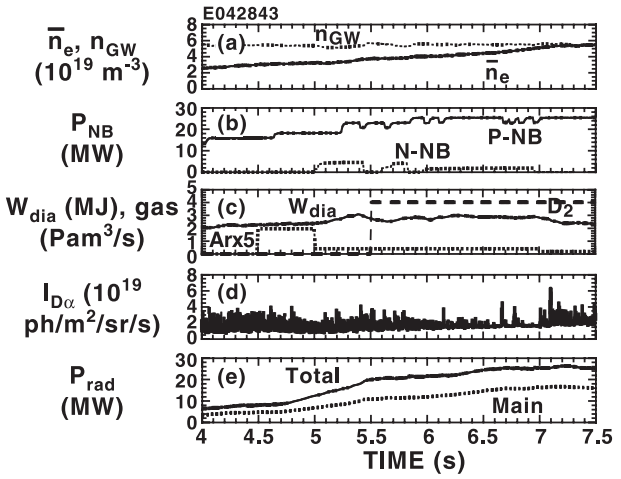

Fig. 2 Typical wave-forms in high density and high radiation loss plasma with argon injection. (a) Solid and dotted lines show line averaged electron density ($\bar{n}_e$) and Greenwald density (n_{GW}), respectively. (b) Solid and dotted lines show injected powers from positive and negative ion based neutral beams (P-NB and N-NB). (c) Solid line shows stored energy (W_{dia}). Dotted and dashed lines show Ar and D_2 puffing rates, respectively. (d) D_α emission intensity from the divertor region. (e) Solid and dashed lines show total radiation loss power and radiation loss power from the main plasma, respectively.

MA and the toroidal magnetic field of B_T = 3.6 T as shown in Fig. 2 [6]. Argon was puffed from t = 4.5 s and penetrated into the plasma with a time delay of 0.2 – 0.3 s. The neutral beam (NB) heating power of P_{NB} = 20 – 30 MW was injected from positive and negative ion based NBs (P-NB and N-NB). The line averaged electron density ($\bar{n}_e$) increased and reached to

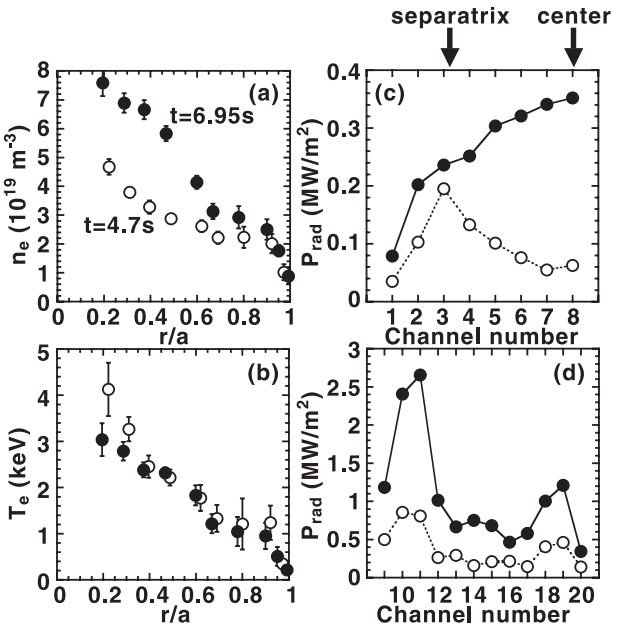

Fig. 3 (a) Electron density and (b) electron temperature profiles before (t=4.7 s : open circles) and after (t=6.95 s : closed circles) the argon penetration. Radiation profiles for (c) main plasma region and (d) divertor region before (t=4.7 s : open circles) and after (t=6.95 s : closed circles) the argon penetration.

the Greenwald density (n_{GW}), which is empirical scaled density for high density disruptive limit, around t = 7.5 s. The stored energy (W_{dia}) was almost kept at constant value and confinement degradation at high density was suppressed by high-field-side pellet injection, argon injection and small D_2 gas-puffing until n = 1 mode appeared at t = 7.1 s. The confinement degradation is observed in many machines when the density is increased by large D_2 gas-puffing. The edge localized mode (ELM) observed in the D_α emission intensity (I_{D_α}) became small during t = 6.5 – 7 s. The radiation losses (P_{rad}) in both main and divertor plasmas were enhanced after argon injection. At t = 6.95 s, the total radiation loss power reached up to 90 % of the heating power at $\bar{n}_e/n_{GW}$ = 0.92 with high confinement enhancement factor of 0.96 over the IPB98 (y,2) ELMy H-mode scaling.

A peaking of the electron density (n_e) profile with the ITB and a flattening of the electron temperature (T_e) profile were observed as shown in Figs. 3(a) and 3(b). The profile of the soft x-ray intensity was also peaked in the main plasma. The radiation had a hollow profile before the argon penetration in the main plasma as shown in Fig. 3(c). After the argon penetration, the central radiation was increased. The divertor radiation was enhanced in the wide region as shown in Fig. 3(d).

3. Methods of analyses

In the main plasma, the profile of the total argon density (n_{Ar}) summed over all ionization states was estimated using a 1-D impurity transport code, where the diffusivity (D) and the convection velocity (v) were determined by fitting the calculated soft x-ray profile to the measurement [2]. The argon radiation coefficient in the soft x-ray range was taken from the ADAS database [7] considering the JT-60U diagnostic setup (the energy range of 2.7 – 20 keV). The absolute value of n_{Ar} was determined by the radiation loss in the central region. The radiation loss from argon was evaluated using the radiative cooling rate calculated in Ref. [8] (ADPAK). The intrinsic impurity carbon density (n_C) was estimated using the 1-D transport code based on the C^{6+} density measured with charge exchange recombination spectroscopy (CXRS). The radiation loss from carbon was also evaluated using ADPAK. In these analyses, the measured parameters of the background plasma such as n_e and T_e were used.

The impurity transport was modeled using the 2-D fluid code UEDGE [5] in the divertor and SOL plasmas. Since detailed background plasma parameters were not measured in the divertor and SOL plasmas, these parameters were also calculated in the UEDGE code consistently with impurity and neutral behavior. In the UEDGE calculation, the boundary conditions at the core-edge (96 % of magnetic flux) were the bulk ion density of 1.5×10^{19} m^{-3} and the power escaping from core to edge of 14 MW divided equally between ions and electrons. The anomalous diffusion coefficients were all taken to be 1.0 m^2/s for the thermal diffusivity and 0.25 m^2/s for the bulk particle diffusivity. The impurity diffusivity was set to be 1.0 m^2/s without the convection velocity. The carbon yield rate was set to be a Haasz yield for both physical and chemical sputtering. The Ar^{15+} density at the core-edge boundary was scanned in the range of $0.5 - 3 \times 10^{16}$ m^{-3}. Recently, drift effects were included in the UEDGE code [9]. However, the drift effects were not included in this modeling. The impurity ionization, radiation and recombination rates came from ADAS rates for carbon and impurity transport code STRAHL [10] for argon.

4. Results of analyses

4.1 Calculations of 1-D transport code and UEDGE code

Impurity transport was analyzed at $t = 6.95$ s in the discharge shown in Fig. 2. The C^{6+} density measured with CXRS indicated a flat profile in the region of $r/a < 0.8$ as shown in Fig. 4(a). In order to reproduce the flat density profile, $D = 1.0$ m^2/s and $v = 0$ m/s were assumed. The density profile calculated in the 1-D transport code is also shown in Fig. 4(a). The calculated C^{6+} density profile was consistent with the measured profile. Figure 4(b) shows the radiation profile calculated from the n_C profile shown in Fig. 4(a). The radiation from carbon impurity was localized in the edge region. The calculated n_{Ar} is shown in Fig. 4(c), where $D = 1.0$ m^2/s and $v = D \cdot \nabla n_e/n_e$ in the region of $r/a \geq 0.65, v = 2 \times D \cdot \nabla n_e/n_e$ in the region of $r/a < 0.65$ were assumed to fit the calculated soft x-ray profile to the measured one. The large inward convection velocity of about −8 m/s was assumed at $r/a \sim 0.6$ due to strong density ITB. In the central region, Ar^{18+}, Ar^{17+} and Ar^{16+} were main contributors and their density ratios were estimated to be 40 %, 40 % and 20 %, respectively. The n_{Ar} profile was more peaked by a factor of 2 than the n_e profile. The radiation from argon impurity was peaked in the central region as shown in Fig. 4(d).

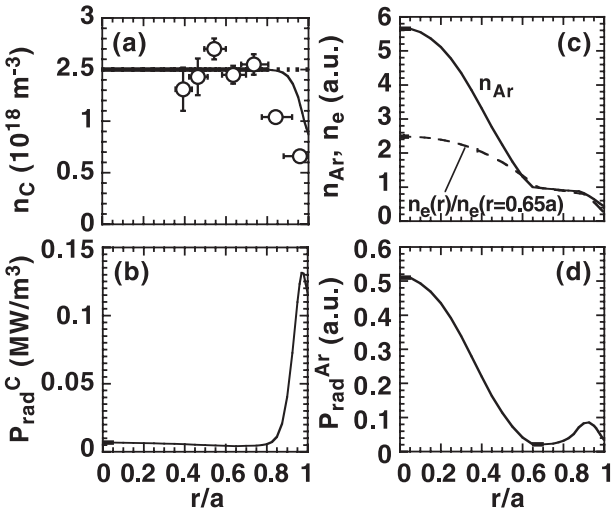

Fig. 4 (a) Carbon density profiles. Circles show the measured C^{6+} density. Solid and dotted lines show the calculated C^{6+} density and total carbon density, respectively. (b) Carbon radiation profile. (c) Solid line shows total Argon density profile. Electron density profile is also shown by dashed line for comparison. Both profiles are normalized at $r/a = 0.65$. (d) Argon radiation profile.

The total radiation loss power calculated with the UEDGE code increased from 6.6 to 8.4 MW by increasing the ratio of n_{Ar}/n_e at the core-edge boundary $(n_{Ar}/n_e)_{core-edge}$ from 0.14 to 0.93 %. The radiation from argon increased from 0.3 to 3.2 MW and the radiation from carbon decreased from 5.7 to 4.7 MW with increasing $(n_{Ar}/n_e)_{core-edge}$. The radiation from deuterium was almost constant ($\sim$ 0.6 MW) and had a small contribution to the total radiation. During this $(n_{Ar}/n_e)_{core-edge}$ scan, n_e and T_e at the outer strike point

decreased from 2.6×10^{20} to 1.9×10^{20} m^{-3} and from 2.7 to 1.3 eV, respectively, with increasing $(n_{Ar}/n_e)_{core-edge}$. The detachment process was gradually progressed at the outer divertor. On the other hand, the inner divertor was detached and n_e and T_e at the inner strike point were in the ranges of $1.8 - 2.8 \times 10^{19}$m^{-3} and 0.68 – 0.72 eV, respectively. The increase in radiation was related to the decrease in n_e and T_e at the outer divertor. At $(n_{Ar}/n_e)_{core-edge} = 1\,\%$, n_e at the outer strike point was largely decreased to 7.2×10^{19} m^{-3} indicating the detachment. At the same time, T_e at the outer strike point was decreased to 1 eV. The total radiation largely increased to 9.7 MW, where the radiations from both carbon and argon were increased to 5.1 MW and 4 MW, respectively. The ratio of the radiation from argon to the total radiation reached to 40 %

4.2 Comparison of radiation profile between measurement and calculation

Figure 5 shows comparison of the radiation profile between measurement and calculation (a) in the main plasma region and (b) in the divertor region. Here, the calculated results of 1-D transport code with argon and carbon were used for the main plasma and the UEDGE calculation result with $(n_{Ar}/n_e)_{core-edge} = 0.75\,\%$ was used for the SOL plasmas in Fig. 5(a). In Fig. 5(b), the UEDGE calculation results with $(n_{Ar}/n_e)_{core-edge} =$ 0.14, 0.75 and 1 % were used together with the 1-D transport results with carbon and argon. Absolute n_{Ar} was determined by adjusting the calculated radiation summed over the 1-D transport and UEDGE results to the measurement at the center bolometer chords (ch 8). In the line integral of the calculated radiation, size of the sight line was considered. The value of n_{Ar} was estimated to be about 1.6 % of n_e in the central region and 0.7 % of n_e in the edge region. The calculated radiation loss was more peaked than the measurement in the main plasma region as shown in Fig. 5(a). When possible misalignment of the sight lines was considered (half channel), the variation of the radiation loss was relatively large in the edge region (ch 4). However, the calculated radiation profile was still peaked. It is necessary to evaluate combination of D and v for satisfying both soft x-ray and radiation profiles in future work. Furthermore, the edge channels (ch 1-3) were much smaller than the measurement. The radiation in the SOL plasma could be larger than the present modeling. In the high triangularity configuration, the large radiation at edge channels viewing the SOL plasma was often observed [11]. Since effect of secondary sepratrix is stronger in this configuration near upper inside corner, this effect on the radiation should be also investigated in future work.

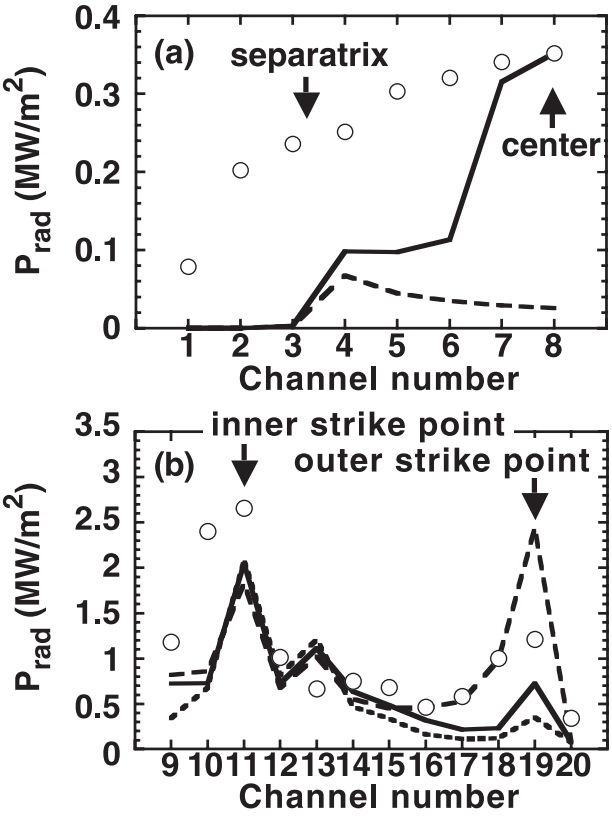

Fig. 5 Comparison between calculated radiation profile and measured one in (a) the main plasma region and (b) the divertor region. Circles show the measurements. (a) Solid line shows the calculated radiation profile summed over the radiations from 1-D transport code results with both carbon and argon and from UEDGE result with $(n_{Ar}/n_e)_{core-edge} = 0.75\,\%$. Dotted line shows the calculated radiation profile summed over the radiations from 1-D transport code result with carbon and UEDGE result with $(n_{Ar}/n_e)_{core-edge} = 0.75\,\%$. (b) Dashed, solid and dotted lines show the radiation profile calculated using UEDGE results with $(n_{Ar}/n_e)_{core-edge} = 1\,\%$, 0.75 % and 0.14 %, respectively.

The divertor radiation had peaks at both strike points (ch 11 for inner and ch 19 for outer divertor) as well as the measurement. The peak at the inner strike point was almost constant even when $(n_{Ar}/n_e)_{core-edge}$ was increased. The peak at the outer strike point was largely enhanced with $(n_{Ar}/n_e)_{core-edge} = 1\,\%$ and was larger than the peak at the inner strike point. The calculated radiation with $(n_{Ar}/n_e)_{core-edge} = 0.75\,\%$, which was consistent with $(n_{Ar}/n_e)_{core-edge}$ calculated using 1-D transport code, was consistent with the measurement at the inner strike point within the ambiguity ($\pm$ 15 %) of the measurement. At the outer strike point, the effect of misalignment of the sight lines was large due to strong localization of the radiation in front of the outer diver-

tor plate. Therefore, when possible misalignment (half channel) was considered, the radiation loss at the outer strike point increased to the same value as the measurement. On the other hand, the radiation in the divertor region (ch 9&10 for inner and ch 17&18 for outer divertor) was smaller than the measurement, indicating that the calculated radiation was localized around the strike points compared with the measurement.

5. Summary

Impurity transport was modeled using a 1-D transport code for the main plasma and the 2-D fluid code UEDGE for the divertor and SOL plasmas in the high β_p ELMy H-mode plasma with argon injection on JT-60U. The calculated radiation profile was more peaked than the measurement in the main plasma, and the calculated radiation was much smaller than the measurement in the edge region. The expanded radiation zone into the wide SOL plasma should be investigated in future work. The radiation calculated with the UEDGE code was localized around the strike points compared with the measurement. The systematic parameter scan such as diffusivity and recycling coefficient is necessary to reproduce the measured radiation profile as well as the considering the drift effects.

Acknowledgements

The authors wish to thank Dr. N. Oyama for establishment of the computer system for UEDGE code and Dr. Y. Kamada for the support on this study.

References

[1] H. Takenaga *et al*., Fusion Technol. **42**, 327 (2002).
[2] H. Takenaga *et al*., Nucl. Fusion **43**, 1235 (2003).
[3] G.D. Porter *et al*, Phys. Plasma **7**, 3663 (2000).
[4] K. Shimizu *et al*., J. Nucl. Mater. **220-222**, 410 (1995).
[5] T.D. Rognlien *et al*., Contrib. Plasma Phys. **34**, 362 (1994).
[6] H. Takenaga *et al*., in Proc. 20th Int. Conf. on Fusion Energy 2004 (Vilamoura, 2004) EX/6-1.
[7] H.P. Summers, JET-IR 06, JET Joint Undertaking, Culham (1994).
[8] D.E. Post *et al*., Atomic Data and Nuclear Data Tables **20**, 397 (1977).
[9] G.D. Porter *et al*., J. Nucl. Mater. **313-316**, 1085 (2003).
[10] K. Behringer, "Description of the Impurity Transport Code STRAHL", JET Report R (87) 08 (1987).
[11] S. Konoshima *et al*., J. Nucl. Mater. **313-316**, 888 (2003).